

NJC

Accepted Manuscript



This is an *Accepted Manuscript*, which has been through the Royal Society of Chemistry peer review process and has been accepted for publication.

Accepted Manuscripts are published online shortly after acceptance, before technical editing, formatting and proof reading. Using this free service, authors can make their results available to the community, in citable form, before we publish the edited article. We will replace this *Accepted Manuscript* with the edited and formatted *Advance Article* as soon as it is available.

You can find more information about *Accepted Manuscripts* in the [Information for Authors](#).

Please note that technical editing may introduce minor changes to the text and/or graphics, which may alter content. The journal's standard [Terms & Conditions](#) and the [Ethical guidelines](#) still apply. In no event shall the Royal Society of Chemistry be held responsible for any errors or omissions in this *Accepted Manuscript* or any consequences arising from the use of any information it contains.



NJC

ARTICLE

Facile synthesis of Sn/MoS₂/C composite as anode materials for lithium-ion batteries with outstanding performance

Hongqiang Wang,^{ab} Qichang Pan,^a Jing Chen,^a Yahui Zan,^a Youguo Huang,^{*a} Guanhua Yang,^a Zhixiong Yan,^a and Qingyu Li^{*a}

Received 00th January 20xx,
Accepted 00th January 20xx

DOI: 10.1039/x0xx00000x

www.rsc.org/

A facile strategy for preparing novel Sn/MoS₂/C composite has been developed via a simple hydrothermal route and then annealed in Ar atmosphere. The synthesis of layer-structure MoS₂ and amorphous carbon can effectively restrict the volume change of Sn during the charge and discharge process. While the Sn/MoS₂/C composite is evaluated as anode materials for lithium-ion batteries, which exhibits a stable and high reversible capacity of 707 mA h g⁻¹ at 500 mA g⁻¹ after 100 cycles. The significant improved Li ion storage and stable capability are attributed to the layer-structure MoS₂ nanosheets and the amorphous carbon coating layer, alleviating the large volume changes of Sn and enhancing the electron and Li ion diffusion transport in the composite.

1. Introduction

Lithium ion batteries (LIBs), have been widely considered as a promising power source for full electric vehicles and hybrid vehicles.¹ However, the current commercial anode materials of graphite can't meet the next generation of high-performance LIBs due to its low theoretical specific capacity (372 mA h/g).² As well as we known, the anode materials being an essential component of the LIBs, significantly influences all the aspects of the performance for LIBs. So the next generation of high-performance LIBs of anode materials should possess a higher capacity in comparison to the commercial graphite.³ In recent years, Alloy-based anode materials have attracted attention because of their considerable higher theoretical capacity than that of graphite. For example, Li-Si alloy and Li-Sn alloy can achieve a capacity of 4200 mA h/g and 993 mA h/g, respectively.^{4,5} Among all the alloy-based anode materials, metallic tin is one of the most promising anode materials for next generation high-performance LIBs due to its not only has high theoretical capacity and electronic

conductivity but also has moderate operating voltage.⁶⁻⁸ Unfortunately, the huge volume changes (about 300%) and severe pulverization during the charge and discharge process cause the shortened cycle ability and cycle life, which has been limited applications in high-performance LIBs.^{9,10}

To overcome these problems, some effective efforts have been made to improve the structural stability. One approach is constructing hybrid composites consisting of nanosized Sn and carbon that have been widely employed to reduce the volume expansion of Sn, such as design a Sn@C nanocomposites,^{11,12} Sn nanoparticles embedded into carbon matrix¹³⁻¹⁶ and Sn-Graphene nanocomposites.¹⁷⁻²² These carbon and graphene can not only provide spaces to buffer the mechanical stress induced by the volume change of the Sn nanoparticles but also enhance the electronic conductivity of the composites, resulting in significantly improved cycling performance and rate capability. Another approach involves the doping of inactive phase, such as Sn-Ge alloy,²³ Cu-Sn thin film²⁴ and Ni-Sn alloy.^{25,26}

Recently, MoS₂, a transition metal sulfide with graphene-like layered structure, has been discovered with high reversible capacity in the range of 900 - 1200 mA h g⁻¹ as the anode materials for LIBs.²⁷⁻²⁹ However, MoS₂ nanosheets are vulnerable to easy restacking due to its structural weakness from its 2D structure, and that result in poor cycle life.^{30,31} To overcome this obstacle, particles with various sizes are introduced as spacers between nanosheets, that can enhance the cycle stability.^{32,33}

In this paper, we reported a facile process to synthesize Sn/MoS₂/C composite. Sn/MoS₂/C

^a Guangxi Key Laboratory of Low Carbon Energy Materials, School of Chemical and pharmaceutical Sciences, Guangxi Normal University, Guilin, 541004, China.

^b Hubei Key Laboratory for Processing and Application of Catalytic Materials, College of Chemical Engineering, Huanggang Normal University, Huanggang 438000, China

Corresponding authors
E-mail addresses:

* Qingyu Li, lqy62@126.com,

* You-Guo Huang, huangyug72@163.com

composite was prepared by hydrothermal route and then heat treat process. The products were characterized by XRD, SEM, and TEM. The results indicate that the Sn dispersed in MoS₂ and amorphous carbon. Furthermore, higher capacity and better cycling stability were displayed at a current density of 500 mA g⁻¹ compared to conventional powder electrode. This good performance is attributed to cooperate with the MoS₂ and amorphous carbon, accommodating the large volume changes of Sn.

2. Experimental

2.1 Material synthesis

In a typical synthesis, 2.25 g of Na₂MoO₄·2H₂O and 3 g NH₂CSNH₂ were dissolved in 400 ml deionized water, and then 7.5 g of glucose was added into the solution, finally, 3.4 g of Na₂SnO₃·3H₂O and 6 g NH₂CONH₂ were also added into the solution. After stirring for a few minutes, the obtained solution was transferred into a 500 ml Teflon-lined stainless steel autoclave and sealed tightly, heated at 220 °C for 24h. After cooling naturally, the black precipitates were collected by filter, and then washed with deionized water three times, dried oven at 80 °C for 12 h. The obtained products were annealed in a conventional tube furnace at 700 °C for 4 h under Ar atmosphere. Then the Sn/MoS₂/C composite was obtained. For comparison, Sn/C composite was also synthesized by hydrothermal method and without introduced MoS₂ at the same conditions.

Characterization of structure and morphology

The morphology of the composite was observed by a field-emission scanning electron microscope (SEM, Philips, FEI Quanta 200 FEG) and transmission electron microscope (TEM, JEOL-2100). The phase of the composite was conducted by X-ray diffraction (XRD, Rigaku D/max 2500) with Cu K α radiation at 40 kV and 40 mA. The crystal and composition were characterized by laser Raman spectroscopy (Jobin Yvon, T6400). X-ray photoelectron spectroscopy (XPS) experiments were carried out using an AXIS ULTRA DLD instrument, using aluminum K α X-ray radiation during the XPS analysis. The carbon content was determined from thermogravimetric analysis (TGA) (Nitzsch STA 449 C) at a heating rate of 5 °C min⁻¹. The exact Mo:Sn molar ratio in the composite was also measured by inductively coupled plasma optical emission spect-roscopy (ICP-OES, Agilent 730). The result measured for the presence of Mo and Sn element (molar ratio: Mo : Sn = 0.0093: 0.013) by TCP-OES.

Electrochemical measurements

Electrochemical measurements were performed using a CR2025 type coin cell with Li metal as the counter

electrode, a polypropylene film (Celgard 2400) as a separator, and 1 M LiPF₆ dissolved in a mixture of ethylene carbonate (EC) and dimethyl carbonate (DMC) (1:1, v/v) was used as the electrolyte. the working electrodes prepared by 80 wt % active materials, 10 wt % Super P as the conductive agent, 10 wt % polyvinylidene fluoride (PVDF) as the binder in an N-methyl pyrrolidinone (NMP) solution. The slurry was pasted on to a copper foil and completely dried before used, and the working electrode with active material loading of around 1.0 mg cm⁻². The charge and discharge cycles were carried out on a battery measurement system (LAND, BT2013A, Wuhan, China) at various current densities in the cut off voltage range of 3.00 V to 0.01 V versus Li/Li⁺ at room temperature. Cyclic voltammograms (CVs) measurements were carried out on electrochemical workstation (IM6, Germany) over the potential range of 3.0 to 0.01 V at a scan rate of 0.1 mV s⁻¹. Electrochemical impedance spectroscopy measurements were performed using a electrochemical workstation by employing an ac voltage of 5 mV amplitude in the frequency range 10 mHz - 100 kHz.

3. Results and discussion

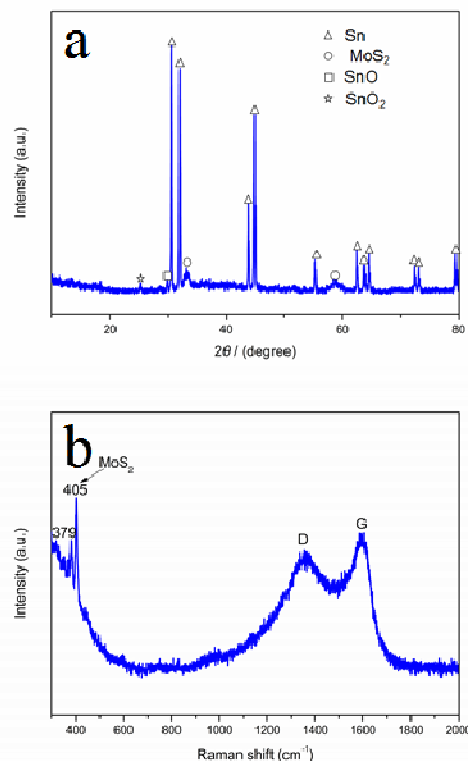


Fig. 1 (a) XRD pattern of Sn/MoS₂/C composite and (b) Raman spectrum of Sn/MoS₂/C composite.

The components of the as-prepared Sn/MoS₂/C composite were characterized by X-ray powder diffraction (XRD), as shown in Fig. 1a. XRD phase analysis reveals, the diffraction peaks at (200), (101), (220), (211), (301), (112), (400), (321), (420), (411) and (312) were observed, which was matched well with metal tin, and the XRD pattern also shows two peaks at (100) and (110), which can be attributed to MoS₂.³⁴ In addition, there is a small amount of SnO₂ and SnO impurity existing in the as-prepared composites. The occurrence of Sn oxides can be explained by follow reasons: (i) the thermal treatment at 700 °C in Ar atmosphere that the carbon not completely reduction of the tin oxides; (ii) part of tin metallic particles, probably oxidized due to the contact with air during the sample handling. Raman spectra of the Sn/MoS₂/C composite (Fig. 1b) displays two characteristic peaks of MoS₂ at 379 and 405 cm⁻¹, the difference (Δ) between these two Raman peaks can be used to identify the number of MoS₂ layers. Therefore, the obtained Δ value is 26 cm⁻¹ in the Sn/MoS₂/C composite, indicating that MoS₂ has a few-layer structure in the composite.³⁵ Moreover, two prominent peaks at ~1345 cm⁻¹ (D-band) and ~1573 cm⁻¹ (G-band), respectively, which are typical bands of carbonaceous. These above mentioned results further confirm that the obtained composite comprises MoS₂ and carbon.

The Sn/MoS₂/C composite is also confirmed by using X-ray photoelectron spectroscopy analysis (XPS) (as shown in Fig. S1). Fig. S1a shows the survey XPS spectrum of Sn/MoS₂/C composite, which suggests the presence of C, O, Mo, S and Sn elements. As shown in Fig S1b, Sn 3d_{3/2} and Sn 3d_{5/2} were observed to be around 495.7 and 487.3 eV, respectively. The result indicates that Sn element detected exists as Sn⁴⁺ state, which indicates the presence of SnO₂ on the surface of Sn/MoS₂/C composite that may be the surface of the Sn have been oxidized in air during the analysis. In addition, S 2s, Mo 3d_{5/2} and Mo3d_{3/2} were located at 225.9, 228.5 and 231.7 eV, respectively, as shown in Fig. S1c. The peaks of S 2p were resolved into S 2p_{1/2} and S 2p_{3/2} shown in Fig.S1d. Such Mo peak corresponded to +4 oxidation state, suggesting that presence of MoS₂ in the composite. So all these indicating that we successfully prepared Sn/MoS₂/C composite.

The content of Sn in the Sn/MoS₂/C composite and Sn/C composite were confirmed by the thermo-gravimetric analysis (TGA) in dry air. The TGA curves of Sn/MoS₂/C composite and Sn/C composite are shown in Fig. 2. The one continuous weight loss in the range of approximately 150-350 °C for the Sn/MoS₂/C composite is attributed to the oxidation of MoS₂ to MoO₃, the Sn to SnO₂ and the decomposition of amorphous.³⁶ Based on the TG result and the ICP-OES result of the Mo : Sn molar ratio of 0.0093 : 0.013, the mass fraction of Sn, MoS₂ and C in Sn/MoS₂/C composite can be calculated around 34 %, 33 % and 33 %, respectively. Based on the TG result, the mass fraction of Sn and C in Sn/C composite can be calculated

around 39.95% and 60.05%.

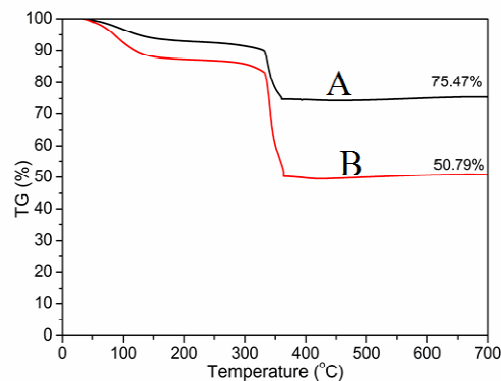


Fig. 2 TG curves of the (A)Sn/MoS₂/C composite and (B) Sn/C composite.

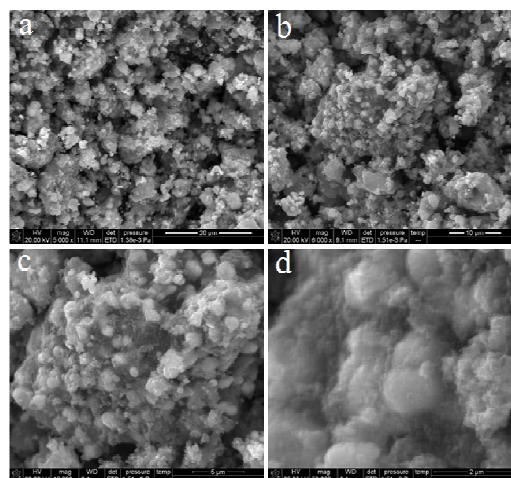


Fig. 3 SEM images of Sn/MoS₂/C composite.

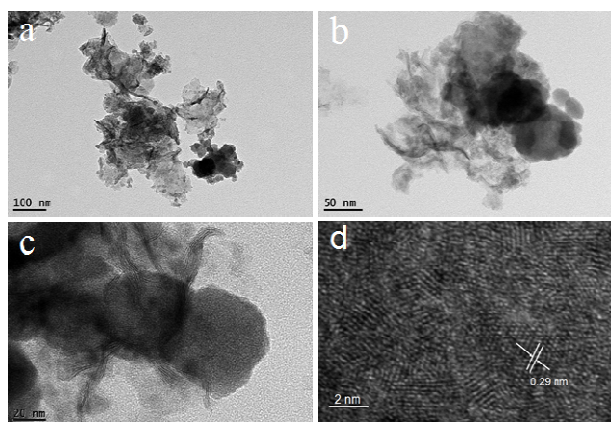


Fig. 4 TEM images of Sn/MoS₂/C composite.

The morphology of the Sn/MoS₂/C composite was shown in a low magnification SEM images (Fig. 3). The Sn/MoS₂/C composite composed of irregular particles with nonuniform sizes, it can be seen that the obtained powders with an average size of about 5 μm and unevenly dispersion. In addition, we also can see that some Sn nanoparticles about a few hundred nanometers embedded in the matrix (Fig. 3 c), and some MoS₂ nanosheets coating the surfaces of the Sn nanoparticles (Fig. 3d). The energy dispersive spectrometer (EDS) mapping (as shown in Fig. S2) of the as prepared sample demonstrates that Sn nanoparticles and MoS₂ are highly dispersed in the carbon matrix. Besides tin, carbon, molybdenum and sulfur, oxygen was also detected, being consistent with the XRD and XPS results. To further investigate the morphology and structure of Sn/MoS₂/C composite, the composite was further characterized by TEM. The low magnification TEM images (Fig. 4a,b,c) showed dispersive aggregates and the particles size distribution ranged from 50-100 nm of Sn particles were coated by the MoS₂ nanosheets and amorphous carbon, Fig. 4d shows the lattice images of the Sn/MoS₂/C composite, the lattice fringe with measured inter-planar distance of 0.29 nm, which indicating that the composite include Sn. These results suggest that during the hydrothermal process, the Na₂SnO₃ transform into SnO₂ by hydrolysis first and then the MoS₂ generated on the surface or in the surrounding of the SnO₂. After annealed in 700 °C under Ar atmosphere, the SnO₂ was reduced to Sn by carbon. However, the SnO₂ may be prepared before the MoS₂, so the SnO₂ is very easily aggregated to large particles.

The cyclic voltammetry plots of the Sn/MoS₂/C composite is shown Fig. 5 (a), Which is collected at a slow scan rate of 0.1 mV s⁻¹ in a potential window of 0.01 V-3.0 V vs Li⁺/Li. In the first cathodic scan, the peaks located at 0.35V and 0.65V are referenced to the alloying process of lithium into tin forming Li_xSn,³⁷ the peak at the 0.8V could be assigned to the formation of a solid electrolyte interface on Sn/MoS₂/C composite and the cathodic peak at 1.65 V is attributed to the Li intercalation into the layered MoS₂. Turning to the anodic process, a series of peaks between 0.4 V and 0.8 V are assigned to the de-alloying reactions of Li_xSn, and a dominant peak at around 2.35 V can be observed, which is ascribed to the oxidation of Li₂S to form S.³⁸ It can be seen that the plots of the second and third scans are almost overlapped, indicating that good electrochemical reversibility of lithium storage in the Sn/MoS₂/C composite starts from the second cycle. To investigate the lithium ion storage capability of Sn/MoS₂/C composite as an anode for LIBs, galvanostatic charge-discharge cycling of the composite was performed in the voltage of 0.01 to 3.0 V at current density of 500 mA g⁻¹.

The charge and discharge profiles of Sn/MoS₂/C composite in the 1st, 2th, 50th and 100th cycles are displayed in Fig. 5 (b). The shape of the profiles changes little during the charge and discharge cycling, indicating the good reversibility of the Sn/MoS₂/C electrode, which is

consistent with the above CV analysis. Besides, during the charge process, a plateau appeared at around 2.35 V is observed, which is in accordance with the previous CV curves. While during the discharge process, a plateau at around 1.8 V and a gentle slope between 0.2 V and 0.8 V are observed, which also in agreements with the above CV study.

Electrochemical properties of Sn/MoS₂/C composite as anode materials for LIBs were also investigated. Fig. 5 (c) display the cycling performance of Sn/C composite during cycling under a current density at 100 mA g⁻¹ and Sn/MoS₂/C composite during cycling at a current density of 500 mA g⁻¹ between 0.01 V to 3.0 V. As can be seen, during the initial cycles a rapid capacity fade occurs and the initial Coulomb efficiency is relatively low, that may be due to inevitable formation of a solid electrolyte interface (SEI) and the decomposition of the electrolyte, which are common to most Sn-based anode materials. In the subsequent cycles, the Sn/MoS₂/C composite electrode exhibits excellent cycling stability at a current density of 500 mA g⁻¹. Even after 100 cycles at 500 mA g⁻¹, a reversible capacity of 707 mAh g⁻¹ is still retained and the Coulomb efficiency keeps stable at ~98% after the first and second cycles, suggesting that the Sn/MoS₂/C composite electrode reveal a excellent cyclic stability. In contrast, a much lower reversible capacity (301 mAh/g) of the Sn/C composite and a reversible capacity (562 mAh/g) of the MoS₂/C composite is delivered at the end of 100 cycle at current density of 500 mA/g, respectively. Therefore, the Sn/MoS₂/C composite demonstrates remarkably higher reversible capacity and cycling stability, which are ascribed largely to the strong MoS₂ nanosheets. During the charge and discharge process, the MoS₂ nanosheets around Sn particles are very beneficial for the growth of a stable SEI film, leading to excellent cycling stability. As for the MoS₂ nanosheets with excellent mechanical flexibility, they can tightly anchor the Sn particles and effectively buffer the volume change of the Sn during the charge and discharge process.³² However, the electrochemical performance is not better than reported Sn/C^{11,12} or MoS₂-based materials^{32,33} may be due to the Sn particles is too big.

To further evaluate the rate capability, the Sn/MoS₂/C composite electrode is cycling at various current densities ranging from 100 to 2000 mA g⁻¹ over a voltage window of 0.01 to 3.0 V as shown in Fig. 5 (d). During the first twenty cycles under current density of 100 and 200 mA g⁻¹, delivered reversible capacity of 865 mAh g⁻¹ and 772 mAh g⁻¹, and then became stable and also can delivered reversible capacity of 665 mAh g⁻¹, 584 mAh g⁻¹ and 485 mAh g⁻¹ at higher current density of 500 mA g⁻¹, 1 A g⁻¹ and 2 A g⁻¹, respectively. When the current density was reduced to 100 mA g⁻¹ again, a reversible capacity of 870 mAh g⁻¹ was obtained, indicating outstanding rate capability. However, for the Sn/C composite, the discharge capacity were 576 mAh g⁻¹ and 247 mAh g⁻¹ at current density of 100 mA g⁻¹ and 2A g⁻¹, respectively, and when

the current density was reduced to 100 mA g^{-1} again, a reversible capacity of 500 mAh g^{-1} was obtained. All the above results clearly demonstrate the excellent cycle stability and rate capability of the as-prepared Sn/MoS₂/C electrode.

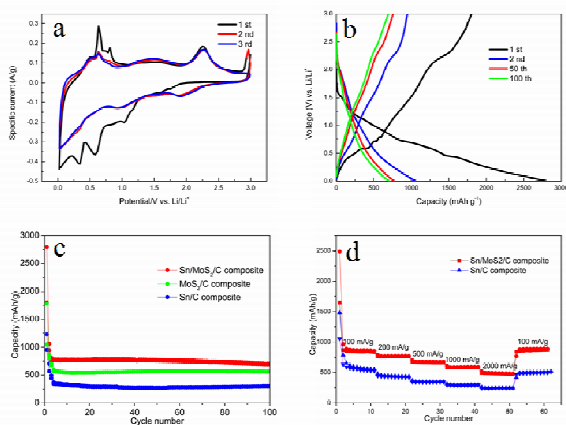


Fig. 5 (a) Cyclic voltammograms of Sn/MoS₂/C composite; (b) galvanostatic charge and discharge profiles of Sn/MoS₂/C composite; (c) Cycle performance of Sn/MoS₂/C composite at current density of 500 mA g^{-1} ; (d) rate capability of the Sn/MoS₂/C composite.

Electrochemical impedance spectroscopy (EIS) measurements were investigated to further identify the resistance of Sn/MoS₂/C composite. Fig. 6 displays the Nyquist plots of Sn/MoS₂/C composite before and after 1st, 5th, 10th and 50th charge-discharge cycles. As can be seen, the five impedance spectra have similar features: a medium-to-high-frequency depressed semicircle and a low-frequency linear tail. The semicircle at high frequency is an indication of SEI resistance (R_{SEI}) and contact resistance (R_{f}), the semicircle across the medium-frequency region represents the charge-transfer impedance (R_{ct}) on the electrode/electrolyte interface, and the low-frequency linear tail corresponds to the Warburg impedance (Z_{w}) associated with the diffusion of lithium ions in the bulk electrode (R_{e}).^{39,40} According to Fig. 6, it can be found clearly that the resistance before cycling was considerably higher than after the 50th cycle, but was closed to the resistance after 1st cycle, which was mainly caused by the lack of electrolyte wetting in the electrode materials before cycling. After the formation of the SEI film and the process of activation during the cycling, the resistance greatly decreased, and the small value of resistance explains the excellent cycling performance and have a rapid Li^+ diffusion. The SEM images of electrode before and after 50 cycles (as shown in Fig S3). It can be clearly seen that the electrode maintain well after 50 cycles, and the Sn particles have not aggregated and still embedded in the MoS₂/C composite. All of these results confirm that the Sn/MoS₂/C composite shows excellent electrochemical performance.

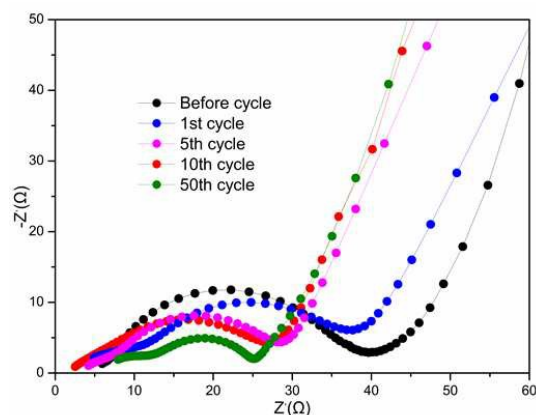


Fig. 6 Nyquist plots of Sn/MoS₂/C composite in the frequency range from 0.01 Hz to 10^5 Hz before and after 1st, 5th, 10th and 50th charge-discharge cycles.

4. Conclusion

In summary, this work has developed a facile method to prepare Sn/MoS₂/C composite by a simple hydrothermal method and then annealed at $700 \text{ }^\circ\text{C}$ for 4h under Ar atmosphere. In this composite, the MoS₂ nanosheets and amorphous carbon can effectively persevere the structural and interfacial stabilization of Sn as well as accommodate the mechanical stress resulting from the severe volume change of Sn during lithium ion insertion/extraction. As a result, excellent cycling stability at high rates (a reversible capacity of 707 mAh g^{-1} is achieved at current density of 500 mA g^{-1} after 100 cycles) and superior rate capability (865 mAh g^{-1} at 100 mA g^{-1} , 772 mAh g^{-1} at 200 mA g^{-1} , $1,665 \text{ mAh g}^{-1}$ at 500 mA g^{-1} , 584 mAh g^{-1} at 1 A g^{-1} and 485 mAh g^{-1} at 2 A g^{-1}) were achieved when Sn/MoS₂/C composite was used as an LIBs anode materials.

Acknowledgements

This work is supported by the National Natural Science Foundation of China (U1401246 and 51364004), and Guangxi Natural Science Foundation (2013GXNSFDA019027).

References

- H. G. Jung, M. W. Jang, J. Hassoun, Y. K. Sun and B. Scrosati, *Nat. Commun.*, 2011, 1527, 1-5.
- J. Z. Chen, L. Yang, Z. X. Zhang, S. H. Fang and S. I. Hirano, *Chem. Commun.*, 2013, 49, 2792-2794.
- Y. Chen, J. Lu, S. Wen, L. Lu and J. M. Xue, *J. Mater. Chem. A*, 2014, 2, 17857-17866.
- M. Ko, S. Chae, S. Jeong, P. Oh and J. Cho, *ACS Nano*, 2014, 8, 8591-8599.

- 5 M. J. Zhou, Y. C. Liu, J. Chen and X. L. Yang, *J. Mater. Chem. A*, 2015, 3, 1068-1076.
- 6 J. Qin, C. N. He, N. Q. Zhao, Z. Y. Wang, C. S. Shi, E. Z. Liu and J. J. Li, *ACS Nano*, 2014, 8, 1728-1738.
- 7 J. Kaspar, C. Terzioglu, E. Lonescu, M. Graczyk-Zajac, S. Hapis, H. Kleebe and R. Riedel, *Adv. Funct. Mater.*, 2014, 24, 4097-4104.
- 8 X. Y. Zhou, Y. L. Zou and J. Yang, *J. Power sources*, 2014, 253, 287-293.
- 9 J. B. Chang, X. K. Huang, G. H. Zhou, S. M. Cui and J. H. Chen, *Adv. Mater.*, 2014, 26, 758-764.
- 10 X. K. Huang, S. M. Cui, J. B. Chang, Y. T. Luo, J. W. Jiang, P. T. Hurlley and J. H. Chen, *Angew. Chem. Int. Ed.*, 2014, 53, 1-5.
- 11 D. N. Wang, X. F. Li, J. L. Yang, J. J. Wang, D. S. Geng, R. Y. Li, M. Cai, T. K. Sham and X. L. Sun, *Phys. Chem. Chem. Phys.*, 2013, 15, 3535-3542.
- 12 W. Ni, Y. B. Wang and R. Xu, *Part. Part. Syst. Charact.*, 2013, 30, 873-880.
- 13 Y. R. Zhong, M. Yang, X. L. Zhou, J. P. Wei and Z. Zhou, *Part. Part. Syst. Charact.*, 2014, 1-8.
- 14 Z. Q. Zhu, S. W. Wang, J. Du, Q. Jin, T. R. Zhang, F. Y. Cheng and J. Chen, *Nano Lett.*, 2014, 14, 153-157.
- 15 J. C. Guo, Z. C. Yang and L. A. Archer, *J. Mater. Chem. A*, 2013, 1, 8710-8715.
- 16 Z. Tan, Z. H. Sun, H. H. Wang, Q. Guo and D. S. Su, *J. Mater. Chem. A*, 2013, 1, 9462-9468.
- 17 C. D. Wang, Y. Li, Y. S. Chui, Q. H. Wu, X. F. Chen and W. J. Zhang, *Nanoscale*, 2013, 5, 10599-10604.
- 18 J. S. Zhu, D. L. Wang, L. B. Cao and T. F. Liu, *J. Mater. Chem. A*, 2014, 2, 12918-12923.
- 19 Z. X. Chen, K. Xie and X. B. Hong, *Electrochim. Acta*, 2013, 108, 674-679.
- 20 P. C. Lian, J. Y. Wang, D. D. Cai, G. X. Liu, Y. Y. Wang and H. H. Wang, *J. Alloy. Compd.*, 2014, 604, 188-195.
- 21 X. S. Zhou, J. C. Bao, Z. H. Dai and Y. G. Guo, *J. Phys. Chem. C*, 2013, 117, 25367-25373.
- 22 X. S. Zhou, Y. X. Yin, L. J. Wan and Y. G. Guo, *J. Mater. Chem.*, 2012, 22, 17456-17459.
- 23 S. F. Fan, X. H. Rui, Q. Y. Yan and H. H. Hng, *J. Mater. Chem. A*, 2013, 1, 14577-14585.
- 24 D. B. Polat, J. Lu, A. Abouimrane, O. Keles and K. Amine, *ACS Appl. Mater. Interfaces*, 2014, 6, 10877-10885.
- 25 K. Zhuo, M. G. Jeong and C. H. Chung, *J. Power sources*, 2013, 244, 601-605.
- 26 J. Liu, Y. R. Wen, P. A. Aken, J. Maier and Y. Yu, *Nano. Lett.*, 2014, 14, 6387-6392.
- 27 X. D. Li, W. Li, M. C. Li, P. Cui, L. H. Chu, H. Y. Liu and G. S. Song, *J. Mater. Chem. A*, 2015, 3, 2762-2769.
- 28 K. Chang, W. X. Chen, H. Li, F. H. Huang, Z. D. Xu, Q. B. Zhang and J. Y. Lee, *J. Mater. Chem.*, 2011, 21, 6251-6257.
- 29 X. S. Zhou, L. J. Wang and Y. G. Guo, *Chem. Commun.*, 2013, 49, 1838-1840.
- 30 C. F. Zhang, H. B. Wu, Z. P. Guo and X. W. Lou, *Electrochem. Commun.*, 2012, 20, 7-10.
- 31 T. Yang, Y. J. Chen, B. H. Qu, L. Mei, D. N. Lei, H. N. Zhang and Q. H. Li, *Electrochim. Acta*, 2014, 115, 165-169.
- 32 Y. Chen, B. H. Song, X. S. Tang, L. Lu and J. M. Xue, *Small*, 2014, 8, 1536-1543.
- 33 Y. Chen, J. Lu, S. Wen, L. Lu and J. M. Xue, *J. Mater. Chem. A*, 2014, 2, 17857-17866.
- 34 Z. Wang, T. Chen, W. X. Chen, K. Chang, L. Ma, G. C. Huang, D. Y. Chen and J. Y. Lee, *J. Mater. Chem. A*, 2013, 1, 2202-2210.
- 35 H. H. Zhao, H. Zeng, Y. Wu, S. G. Zhang, B. Li and Y. H. Huang, *J. Mater. Chem. A*, 2015, 3, 10466-10470.
- 36 Y. Wang, G. Z. Xing, Z. J. Han, Z. X. Huang and H. Y. Yang, *Nanoscale*, 2014, 6, 8884-8890.
- 37 H. Liu, R. Z. Hu, W. Sun, M. Q. Zeng, J. W. Liu, L. C. Yang and M. Zhu, *J. Power Sources*, 2013, 242, 114-121.
- 38 J. M. Jeong, K. G. Lee, S. J. Chang, J. W. Kim, Y. K. Han, S. J. Lee and B. G. Choi, *Nanoscale*, 2015, 7, 324-329.
- 39 R. H. Wang, C. H. Xu, J. Sun, Y. Q. Liu, L. Gao, H. L. Yao and C. C. Lin, *Nano Energy*, 2014, 8, 183-195.
- 40 X. Y. Hou, Y. J. Hu, H. Jiang, Y. F. Li, W. G. Li and C. Z. Li, *J. Mater. Chem. A*, 2015, 3, 9982-9988.

Sn/MoS₂/C composite has been synthesized using a simple hydrothermal method with stable electrochemical performance.

